Computational Modeling of the Electroslag Remelting (ESR) Process Used for the Production of Ingots of High-Performance Alloys

Kanchan M. Kelkar and Suhas.V. Patankar
Innovative Research, Inc., 3025 Harbor Lane North, Plymouth, MN 55447, USA
kelkar@inres.com, patankar@inres.com

Alec Mitchell
Department of Metals and Minerals Engineering, University of British Columbia, Vancouver, BC V6T 1Z4, Canada
alecm@interchange.ubc.ca

Keywords: Computational Modeling, Electroslag Remelting, ESR, Superalloy Ingots

Abstract

The Electroslag Remelting (ESR) process is used for the production of defect-free ingots of high-performance alloys for the manufacture of components in aerospace and land-based turbines. In the present study, a comprehensive computational model for the prediction of the performance of the ESR process is presented for axisymmetric, steady state conditions. Analysis of electromagnetics in presence of Alternating Current determines the distribution of Joule heating and Lorentz forces in the slag and the ingot. Turbulent flow, created by the buoyancy and Lorentz forces, is analyzed by solving the time-averaged mass and momentum conservation equations. Nonuniform turbulent mixing is modeled using the two-equation k-ε model. The temperature fields in the slag and the molten metal region are determined by solving the energy conservation equation. The mathematical formulation accounts for all interactions between the slag and the metal phases and loss of heat to the mold wall in a rigorous manner. A control-volume computational method is used for the solution of the governing equations. The computational model is applied for the analysis of a practical low-melt-rate ESR process of IN718. Detailed plots of the flow, temperature, electromagnetic, and turbulent quantities provide valuable information about the process performance. The predicted pool shape also agrees well with the measured pool profile.

Introduction

The Electroslag Refining process (ESR) is a variant of the group of consumable electrode remelting processes (ESR, VAR, EBR and PAR) for producing ingots of higher quality than that of the original material by means of controlled solidification and chemical refining. Figure 1 shows a schematic diagram of the ESR process that uses a stationary water-cooled mold containing the slag and the ingot. The ESR process involves complex interactions of the electromagnetic, flow, and heat transfer processes, as described by Hoyle (1983). A brief overview of these phenomena is presented here. Passage of an Alternating current (AC) from the electrode to the water-cooled base plate results in Joule heating within the high-resistivity slag. Part of the heat generated in the slag melts the electrode and the droplets of the molten metal descend through the slag to enter the pool of molten metal that is formed under the slag-metal interface. The electrode is continuously advanced into the slag as it melts to build up an ingot of improved structure and composition. The flow of current also produces Lorentz forces due to the interaction of the current density and the self-induced magnetic field. The flow in the slag and the molten pool is driven by Lorentz and buoyancy forces. The flow regime is expected to be turbulent due to the large length scales and the substantial temperature differences.
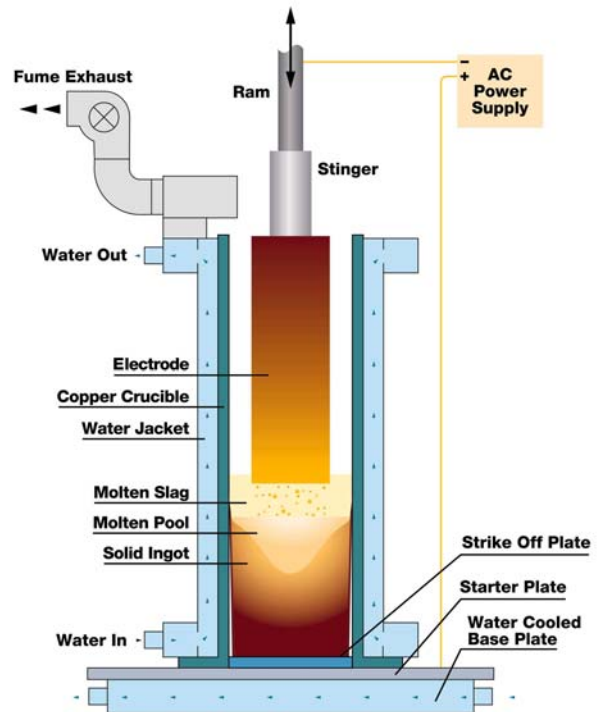
Figure 1: Schematic diagram of the Electroslag Remelting (ESR) process (Courtesy ATI Allvac, 2003).

An important aspect of the ESR process is the transfer of heat to the mold across the slag skin that is formed on the mold surface and that adheres to the circumferential surface of the solidifying ingot. In the slag region, the heat loss to the mold occurs across the slag skin that is in direct contact with the mold surface. As the ingot solidifies, it shrinks away from the mold and the heat is now transferred across the gap formed between the slag skin and the mold surface.

The microstructure of the ingot is controlled by the local solidification time which is, in turn, dependent on the pool profile and the extent of the mushy region. The occurrence of segregation defects is related to solidification contraction, micro-scale flow in the mushy region, and the convective flow in the fully liquid metal. Trial and error approach is inadequate for assessing the relationships between the operational parameters and process performance because of the complexity of the interacting physical phenomena, the high operating and material costs, and the difficulty of obtaining detailed and precise measurements in a high-temperature environment. Mathematical modeling constitutes a scientific and cost-effective approach for developing a fundamental understanding of the governing physical processes and for predicting the effect of various operational parameters on the process performance. A number of studies involving computational analysis of the ESR process are presented in the literature. A brief summary of the relevant studies is presented here. These studies involve computational analysis at various levels such as analysis of only the electromagnetic phenomena or a coupled analysis of all phenomena, analysis of a single region (slag or ingot) or both regions (slag and ingot together), and use of simple (Eddy Viscosity model) or advanced (two equation k-ε model) models for turbulent mixing. Examples of segregated models for flow and heat transfer in the slag are presented by Choudhury and Szekely (1981) and Jardy et al. (1991). The sequence of studies with progressively less restrictive models of electromagnetic, fluid motion, and heat transfer are presented by Dilawari and Szekely (1977, 1978), and Choudhury and Szekely (1980). An analytical model for the prediction of electromagnetic phenomena in ESR and VAR (Vacuum Arc Remelting) processes is presented by Patel (2003). This model constitutes a good basis for verifying the accuracy of the computational solution of the electromagnetic phenomena. A detailed analysis of the heat transfer to the mold for various remelting processes is presented by Yu (1984). Bertram (1997) has described a method for addressing the effect of progressive loss of contact due to the shrinkage of the ingot on the heat transfer to the mold surface during the VAR process.

The present study describes a comprehensive computational model of the ESR process that considers the electromagnetic, flow, heat transfer, and phase change phenomena in a coupled manner. Turbulent mixing in the slag and the molten metal is modeled using the two-equation k-ε turbulence model. The flow and thermal interactions across the slag-pool interface, and heat transfer to the mold surface in presence of the slag skin and the shrinkage of the solidifying ingot are accurately addressed. The model is developed for steady-state conditions that are applicable for long ingots. Note that the computational framework can be readily extended for the analysis of the unsteady process involving a growing ingot. The steady-state computational model has been applied for a practical ESR process for IN718. The results are presented in terms of plots of electromagnetic, flow, and temperature fields along with a comparison of the predicted pool shape with the measured pool profile.

Mathematical Formulation

In the present study, a mathematical model for the ESR process is developed assuming that the process conditions are axisymmetric and steady. Practical ESR processes for casting of cylindrical ingots involve geometries that are axisymmetric and the process conditions are nearly invariant in the angular direction. Therefore, the assumption of axisymmetry enables analysis to be carried out in two dimensions and results in a computationally efficient model that accurately represents the behavior of the physical system. For sufficiently long ingots, the flow and thermal conditions in the pool, the slag, and most of the solidified ingot reach a steady state because they are unaffected by the thermal conditions at the base of the ingot. Thus, steady state analysis enables computationally efficient evaluation of the effect of operating conditions on process performance. The electrode-slag and the slag-metal interfaces are assumed to be flat. Further, the slag-metal interface is internal to the analysis domain. Finally, the frame of reference attached to the slag is used for performing the analysis so that the metal in the solidified ingot region moves at the casting velocity in the axial direction. The computational domain then extends from the top surface of slag to a sufficiently long length within the ingot. The equations governing the various physical phenomena and the corresponding boundary conditions are now described for the entire domain with the physical properties taking appropriate meanings in slag and metal phases.

Electromagnetics

Governing Equations – Practical ESR systems involve flow of current in electrically conducting media so that magnetic field diffusion is the primary electromagnetic phenomenon. Further, the frequency of the AC power is sufficiently high so that the time scale for electromagnetic phenomena is orders of magnitude smaller than that for the casting process. Therefore, electromagnetic analysis is carried for the periodic steady state in which amplitudes of the sinusoidally varying electromagnetic quantities constitute the primary unknowns. Thus, an electromagnetic quantity is represented as a product of a spatially-varying complex amplitude and a sinusoidal time variation as follows.

Periodic Steady State: $\phi = \hat{\phi} e^{j\omega t}$ (1)

For axisymmetric coordinates, the magnetoquasistatic form of Maxwell's equations can be reduced to a single equation for the diffusion of the scalar magnetic flux density as follows.

Magnetic Diffusion: $\nabla \bullet \left(\dfrac{1}{\sigma} \nabla \left(\hat{H}_\theta \mathbf{e}_\theta \right) \right) = j\mu\omega\hat{H}_\theta$ (2)

The current density, Lorentz Force, and Joule heating are then deduced in the following manner.

Current Density: $\hat{\bar{J}} = \bar{\nabla} \times (\hat{H}_\theta \mathbf{e}_\theta)$ (3)

Lorentz Force: $\bar{F}_L = \mathrm{Re}\left(\dfrac{1}{2} \hat{\bar{J}} \times \hat{\bar{B}}_{conjugate} \right)$ (4)

Joule Heating: $S_J = \mathrm{Re}\left(\dfrac{1}{2\sigma} \hat{\bar{J}} \bullet \hat{\bar{J}}_{conjugate} \right)$ (5)

The electromagnetic phenomena influence the temperature fields directly through Joule heating and indirectly through their effect on the flow field due to the Lorentz force.

Boundary Conditions – The radial current is assumed to be zero at the electrode-slag interface (due to the large difference between the electrical conductivities of the electrode and the slag) and at the base of the ingot. This results in the following boundary condition on the magnetic flux density.

Electrode-Slag Interface and Ingot Bottom: $\dfrac{\partial \hat{H}_\theta}{\partial x} = 0$ (6)

On the exposed surface of the slag and at the outer surface of the ingot, the value of the magnetic flux density is specified according to Ampere's law in the following manner:

Exposed Slag Surface: $\hat{H}_\theta(r) = \dfrac{1}{2\pi r} \hat{I}$ (7)

Ingot Circumferential Surface: $\hat{H}_\theta(r) = \dfrac{1}{2\pi R_{Ingot}} \hat{I}$ (8)

In the above equations, $\hat{I}$ denotes the amplitude of the total current entering the slag.

Fluid Motion
Governing Equations - Fluid motion in the slag and the molten pool is driven by the combined action of Lorentz and buoyancy forces. The flow field is represented by the time-averaged form of the mass and momentum conservation equations. The effect of turbulent mixing is accounted for by using a turbulent viscosity. Thus, the corresponding mass and momentum conservation equations are listed below.

Mass Conservation: $\nabla \bullet (\rho\bar{u}) = 0$ (9)

Momentum Conservation:
$\nabla \bullet (\rho\bar{u}\bar{u}) = -\nabla P + \nabla \bullet \left((\mu + \mu_t)\left(\nabla\bar{u} + \nabla\bar{u}^T \right) \right) - \rho\bar{g}\beta\left(T - T_{ref} \right) + \bar{F}_L$ (10)

Note that, in the momentum equation, Boussinesq approximation is used for determining the buoyancy force while the last term represents the Lorentz force.

Boundary Conditions – The no-slip boundary condition is imposed on the region of the mold boundary where the liquid phase (slag or molten metal) is in contact with the mold. The slag is subject to a zero shear stress at the electrode-slag interface and the exposed surface of the slag. In the ingot region, the macro-level flow is assumed to be absent below the immobilization liquid fraction (λ_{immob}) and it corresponds to the solid-liquid interface in the flow calculation. Thus, the liquid metal in the molten pool is subject to the casting velocity at this interface and the velocity of the metal in the mushy and the fully solidified ingot is equal to the casting velocity. These boundary conditions are listed below.

Top Surface: $\dfrac{\partial u_y}{\partial x} = 0$ (11)

Mold Surface: $\bar{u} = 0$ (12)

Solidified Ingot: $u_x = U_{cast}$ for $\lambda \le \lambda_{immob}$ (13)

Energy Conservation
Governing Equations – The temperature distribution in the slag and metal phases is governed by the energy conservation equation. The steady-state form of this equation, with temperature as the primary unknown, is listed below:

Energy Conservation:
$\rho C_P \bar{u} \bullet \nabla T = \nabla \bullet (k\nabla T) + S_J - \rho\bar{u}L\nabla \bullet \lambda$ (14)

Liquid Fraction $\lambda = f\left(\dfrac{T - T_{Solidus}}{T_{Liquidus} - T_{Solidus}} \right)$ (15)

Joule heating created by the current flow appears as the source term in the above equation and it is predominant in the slag region. In the metal region, the release of latent heat, as the liquid metal solidifies, appears as a source term. This source term uses the local liquid fraction λ, which, in turn, is related

3

to the local temperature through a suitable functional relationship. Note that this term is absent in the slag region.

Boundary Conditions – The present study performs analysis of the ESR process for a specified melt rate. Thus, a uniform heat flux is prescribed at the slag-electrode interface. It corresponds to the energy required to heat the electrode from its inlet temperature to the liquidus temperature and any loss of heat that takes place from the exposed surface. The remaining surface of the slag is assumed to lose heat to the surroundings through radiation. The corresponding equations are described below:

$$\text{Electrode-Slag Interface: } -k\frac{\partial T}{\partial x} = \frac{\dot{m}\left(L + \int_{T_{ambient}}^{T_{liquidus}} C_P dT\right)}{A_{electrode}} \qquad (16)$$

$$\text{Exposed Slag Surface: } -k\frac{\partial T}{\partial x} = \varepsilon\sigma\left(T^4 - T_{\sin k}^4\right) \qquad (17)$$

The bottom surface of a sufficiently long ingot is treated as an outflow boundary and conditions at this surface are calculated by extrapolation from within the domain.

The heat loss to the cooling water at the slag-mold interface is calculated by determining an effective heat loss coefficient that accounts for the presence of the slag skin on the ingot surface as described by Yu (1984). The heat loss at the ingot-mold interface accounts for the loss of contact due to the shrinkage of the solidifying ingot away from the mold as proposed by Bertram et al. (1997).

Turbulent Mixing
Governing Equations - The two-equation k-ε model is used to determine the effect of turbulent mixing on the flow and the temperature fields. In this model, the variation of the turbulent viscosity within the region of interest is determined from the local values of the turbulent kinetic energy and turbulent dissipation. These quantities, in turn, are governed by respective convective-diffusive transport equations. Finally, the turbulent conductivity is calculated from the turbulent viscosity using Reynold's analogy. These governing equations are listed below.

Turbulent Kinetic Energy:

$$\nabla\cdot(\rho u k) = \nabla\cdot(\frac{\mu_t}{\sigma_k}\nabla k) + \mu_t G - \rho\varepsilon \qquad (18)$$

Turbulent Dissipation:

$$\nabla\cdot(\rho u \varepsilon) = \nabla\cdot(\frac{\mu_t}{\sigma_\varepsilon}\nabla\varepsilon) + (c_1\mu_t G - c_2\rho\varepsilon)\frac{\varepsilon}{k} \qquad (19)$$

Turbulent Viscosity and Conductivity:

$$\mu_t = c_\mu\frac{\rho k^2}{\varepsilon} \qquad \frac{k_t}{C_P} = \frac{\mu_t}{\text{Pr}_t} \qquad (20)$$

A detailed description of the use of k-ε model for the prediction of turbulent flows is provided by Launder and Spalding (1974).

Boundary Conditions - Since the fully turbulent version of the k-ε model is used, wall functions are employed for specifying boundary conditions for turbulent kinetic energy, turbulent dissipation, shear stress, and heat flux on all the solid surfaces and on the pool boundary corresponding to the immobilization liquid fraction.

Computational Solution

Computational solution of the governing equations is carried using the control volume method of Patankar (1980). It involves use of a main grid for the storage of scalar quantities and a staggered grid for the storage of the velocity components. Discretization equations are constructed by integrating the corresponding differential equations over the individual control volumes. Thus, the discretization equations for a physical variable represent exact conservation of the fluxes over each of the control volumes. The velocity-pressure coupling is handled using the SIMPLER algorithm. Since the discretization equations are nonlinear and coupled, iterations are required to attain convergence.

Two important aspects of the computational method are the treatment of the electromagnetic, momentum, and thermal interactions at the slag-metal interface, and the melting of the electrode and the associated two-phase flow of the metal droplets in the molten slag. First, the harmonic-mean method employed in the computational technique for the calculation of the effective conductance at a control volume face automatically ensures continuity of the radial current, the heat flux, and the shear stress at the slag-metal interface in an accurate manner. Thus, the slag-metal interface is treated in an implicit manner during computational solution. Second, the molten metal droplets formed at the slag-electrode interface are assumed to travel through the slag under thermal equilibrium conditions and are treated as mass and momentum sources in the control volumes in the ingot that lie just below the slag-metal interface and fall under the shadow of the electrode. Further, the heat picked up by the molten metal droplets as they enter the molten pool is treated as a distributed volumetric heat sink in the slag phase to ensure energy conservation. This results in a physically realistic representation of the sensible heating of the molten metal droplets as they fall through the molten slag and enter the metal pool.

Application of the Model

Computational model described above has been incorporated in a commercial software program COMPACT-ESR (2004). This program has been applied for the analysis of a practical ESR process of IN718. Details of the process conditions, computational predictions, and their comparison with experimentally determined pool shape are now presented.

Physical Situation and Computational Details
Table 1 lists the physical properties of the alloy and the slag, and the geometry and the operating conditions used in the present study. The process conditions are typical of a practical low-melt-rate ESR process used for producing superalloy ingots. Note that the conductivity and the specific heat of the metal are assumed to be temperature dependent. However, only their representative values are listed in the table. Finally, the variation of solid fraction with temperature in the mushy region used in this analysis is shown in Fig. 2 (Viswanathan, 2004).

A computational grid of 160(axial)x80(radial) size is used in the analysis. A grid independence study showed that any further increase in the grid size produced a difference of less than 0.1% in the predicted pool size, mushy region, and field variations of the velocity magnitudes and the temperature. Thus, the grid employed in this study is deemed to provide accurate solutions of the governing equations. A total of six hours of computations were required for obtaining a converged solution for the steady-state conditions.
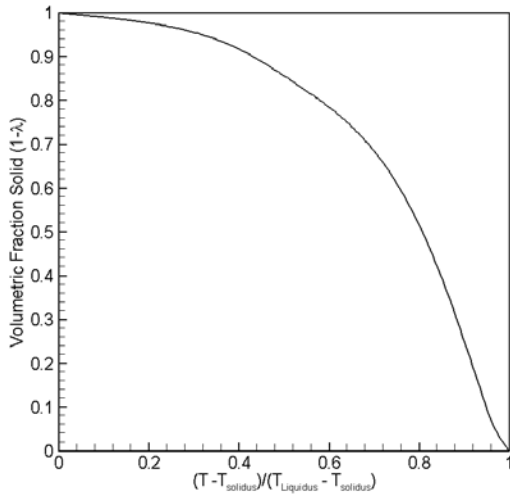
Figure 2: Variation of the volumetric solid fraction with temperature in the mushy region

Table 1: Physical properties and operating conditions used in the analysis of a practical ESR process for IN718

Metal (Alloy 718)	
Density, liquid	7500 kg/m^3
Viscosity, liquid	6x10^{-3}kg/m-s
Liquidus temperature	1623 K
Solidus temperature	1473 K
Latent heat of fusion	2.1x10^5 J/kg
Specific heat, liquid	720 J/kgK
Thermal expansion coefficient, liquid	1.5x10^{-4} K^{-1}
Thermal conductivity,liquid	30.52 W/mK
Thermal conductivity, solid (773 K)	16.72 W/mK
Convective heat transfer coefficient from cooling water to mold	3000 kW/m^{2}K
Electric conductivity, liquid	7.1x10^5 (Ω-m)$^{-1}$
Magnetic permeability	1.257x10^{-6} H/m
Slag	
Density	2800 kg/m^3
Viscosity	2.5x10^{-3} kg/ms
Specific heat	1255 J/kgK
Thermal expansion coefficient	2.5x10^{-4} K^{-1}
Thermal conductivity	6.0 W/mK
Thermal conductivity, slag skin	0.5 W/mK
Geometry	
Slag height	125 mm
Electrode diameter	280 mm
Ingot Diameter	470 mm
Operating condition	
Electric current	6.4 kA
Total Power Dissipation	213 kW
Melt Rate	3.6 kg/min
Emissivity, Exposed Slag Surface	0.5
Sink Temperature, Exposed Slag Surface	400.15 K
Emissivity, Slag Skin Surface	0.4
Temperature of the cooling water	298.15 K

Results and Discussion
The computational model predicts field variations of the electromagnetic, flow, temperature, and turbulent mixing. These variations are presented in the form of field plots of vectors and contours in Figs. 3 to 5. Important aspects of these results are now discussed.

Figure 3(a) shows the contours of magnetic flux density and current density vectors at an instant in the AC cycle. After entering the slag, the current tends to become more uniform due to the low electrical conductivity of the slag. However, as

(a) Magnetic Flux Density and Current Density

(b) Joule Heating and Lorentz Force
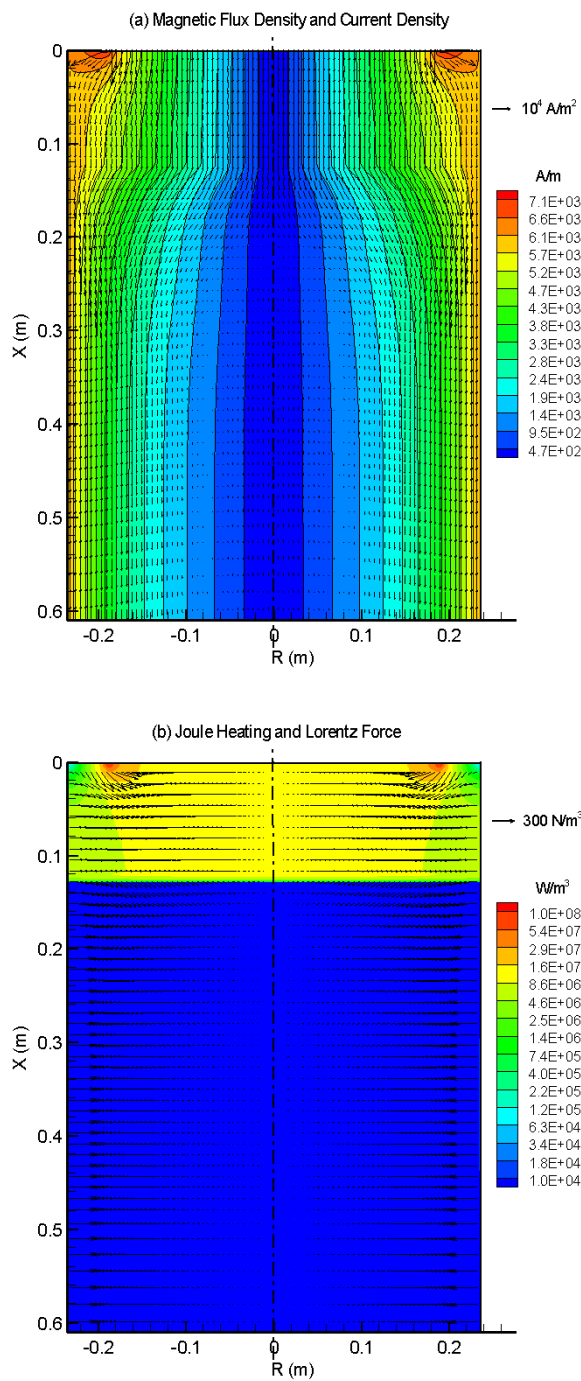
Figure 3: Field variations of the electromagnetic quantities in a practical ESR process for IN718

the current enters the ingot, it migrates radially outwards and flows in a small region near the outer radius of the ingot. This corresponds to the skin effect that occurs in AC power. Figure 3(b) shows the contours of volumetric heating produced by the current and the Lorentz force vectors. The volumetric heating

is concentrated in the slag due to its low electrical conductivity and is highest near the tip of the electrode because the highest current density in the slag occurs at that location. Lorentz force is always directed perpendicular to the current density vectors. It should be noted that, at any spatial location, the Lorentz force does not oscillate with time because it is produced by an interaction of the oscillating

(a) Temperature and Fluid Velocity

(b) Normalized Turbulent Viscosity and Fluid Velocity
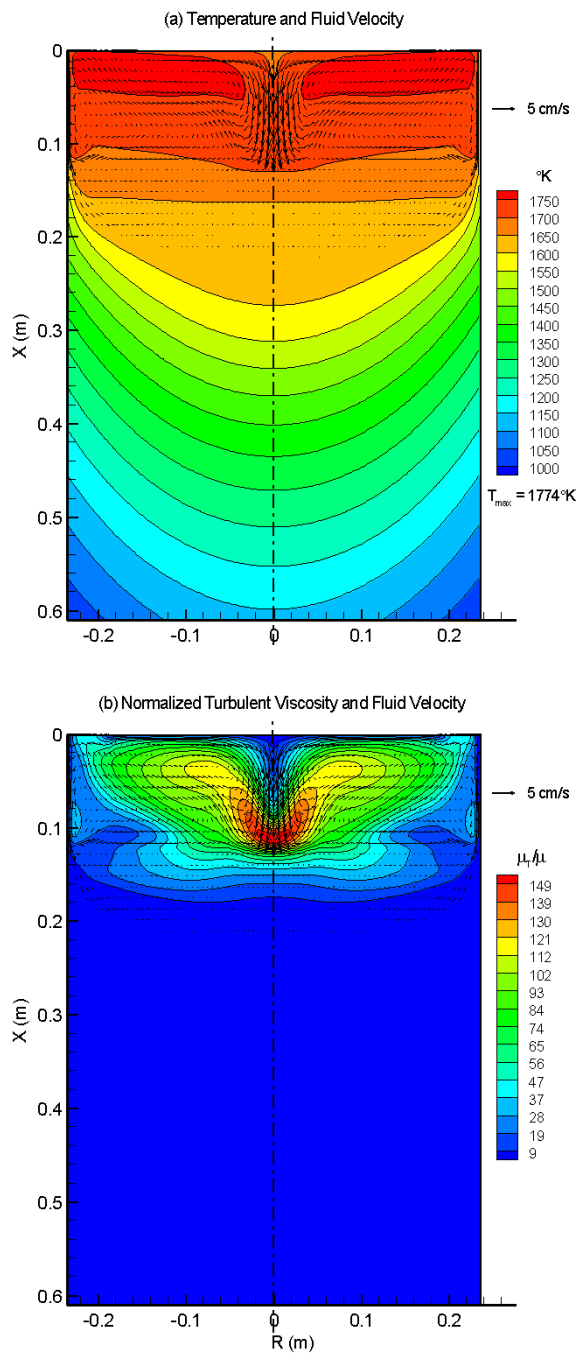
Figure 4: Field variations of velocity, temperature, and turbulent viscosity in a practical ESR process for IN718

current and magnetic fields. In most of the metal region, the Lorentz force is radially inwards. Further, in the slag region and just under the slag-metal interface, it also has an axially downward component due to the radial spreading of the current. Figure 4(a) shows the temperature and the velocity fields in the slag and the ingot regions while Fig. 5(a) shows
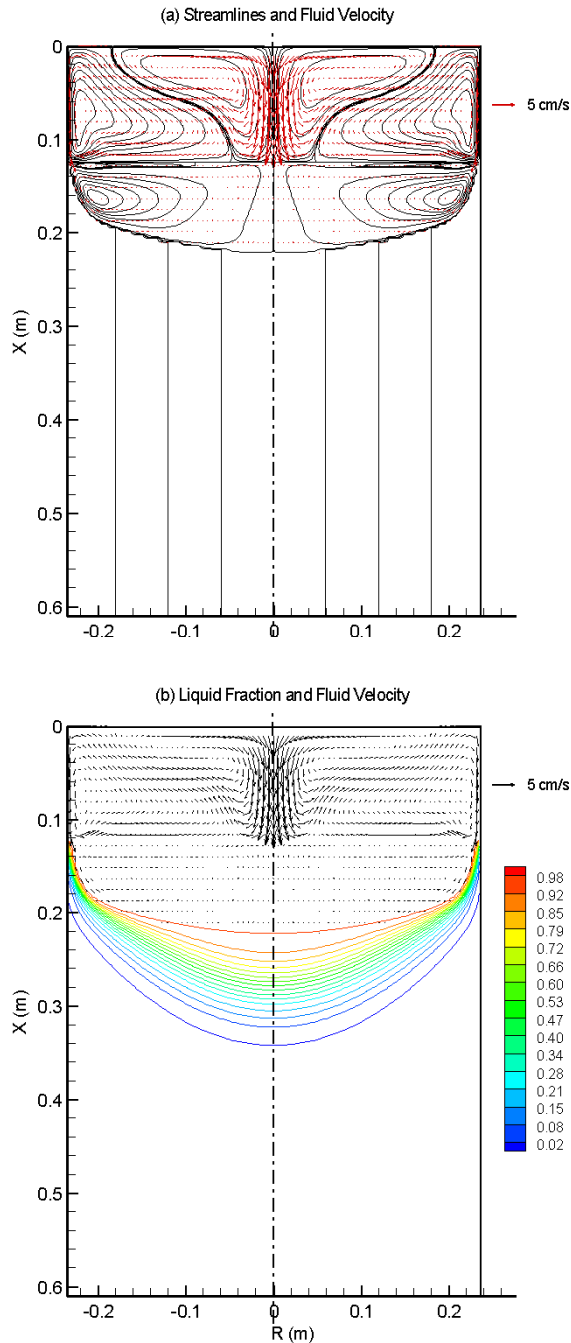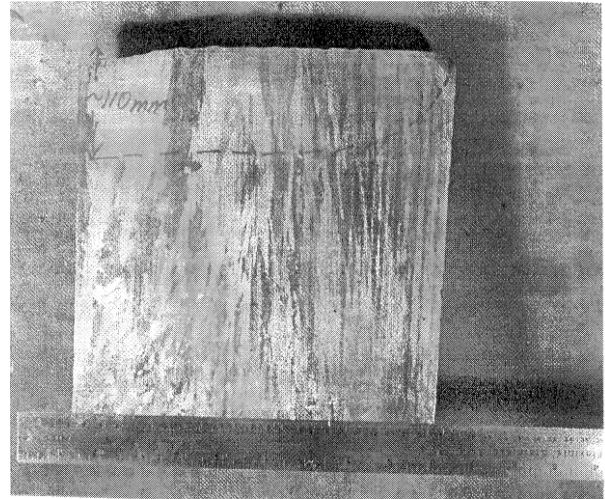
Figure 6: Section of an ESR ingot of IN718 with the marked pool profile.

the streamlines. The slag is seen to be hotter than the metal. Further, the slag region under the electrode is unstably stratified because of the cooling resulting from the melting of the electrode. Therefore, there are two recirculating cells in the slag with a downward motion of the colder slag in the center and over the slag-mold boundary. The metal pool involves a single recirculating cell with downward motion along the pool boundary. The velocities in the slag are an order of magnitude higher than those in the metal. For example, the predicted magnitude of the slag velocity in the annular region at the top surface of the slag is about 1 cm/s while the velocity in the metal pool at midradius under the slag-metal interface is only about 0.15 cm/s. Further, the bulk of the slag is more vigorously mixed as indicated by the larger velocities in that region. Note that the streamlines below the pool boundary (immobilization liquid fraction) are straight vertical lines corresponding to the movement of the solidified metal at the casting velocity. The temperature in the solidified ingot gradually decreases as it loses heat to the mold wall. The extent of turbulent mixing is shown in Fig. 4(b) in terms a plot of contours of turbulent viscosity normalized with the corresponding laminar viscosity in each phase. It is seen that the enhancement in the slag region is much higher than that in the metal region. For example, the enhancement factor for the viscosity in the slag region near the mold is about 65 while the flow in the metal pool in the near-mold region is almost laminar. Finally, the extent of mixing within the slag and the metal varies considerably. Ability to predict nonuniform mixing within the slag and the molten pool is critical for accurate prediction of the transport phenomena in the ESR process.

Figure 5: Streamlines and field variations of liquid fraction and velocity in a practical ESR process for IN718

Figure 5(b) shows the contours of the liquid fraction in the ingot region. The pool profile is judged from the outermost contour of the liquid fraction corresponding to the

7

immobilization liquid fraction of 0.98 or the streamline corresponding to the immobilizaion of the macro-level flow. Due to the low melt rate, there is virtually no standing head of liquid metal and the pool profile in the center of the ingot is nearly flat. The experimentally determined pool profile is marked on a section of the ingot in Fig. 6. Note that the width of the section is larger than the radius of the ingot. The computational model is seen to accurately predict both the pool shape and the pool depth at the ingot center.

Summary and Conclusions

The present study describes a comprehensive computational model for the analysis of electromagnetic, flow, heat transfer, and phase change phenomena in the ESR process for steady, axisymmetric conditions. The model addresses the interactions between the slag and the metal phases, and the heat transfer at the mold interface in a rigorous manner. The model is applied for the analysis of an ESR process for IN718 that is representative of a typical practical low-melt rate process for superalloys. The detailed plots of current distribution, volumetric heating, flow, temperature, turbulent mixing, and liquid fraction fields provide insight into the various physical phenomena that occur in an ESR process. The predicted pool profile also compares well with the measured pool profile. Thus, the computational model constitutes a powerful approach for analyzing the effect of operating conditions on process performance.

Acknowledgements

References

1. G. Hoyle, *Electroslag Processes – Principles and Practice*, Applied Science Publishers, 1983.
2. M. Choudhury and J. Szekely, Modeling of Fluid Flow and Heat Transfer in Industrial-Scale ESR System, *Ironmaking and Steelmaking*, 5, 225-232, 1981.
3. J. Jardy, D. Ablitzer, and J.F. Wadier, Magnetohydrodynamic and Thermal Behavior of Electroslag Remelting Slags, *Metall. Trans. B*, 22B, 111-120, 1991.
4. A. H. Dilawari and J. Szekely, A Mathematical Model of Slag and Metal Flow in the ESR Process, *Metall. Trans .B,* 8B, 227-236, 1977.
5. A.H. Dilawari and J. Szekely, Heat Transfer and Fluid Flow Phenomena in Electroslag Refining, *Metall. Trans. B, 9B,* 77-97, 1978.
6. Choudhury M. and Szekely J., The Modeling of Pool Profiles, Temperature Profiles, and Velocity Fields in ESR Systems, *Metall. Trans. B*, 11, 439-453, 1980.
7. A.D. Patel, Analytical Model for Electromagnetic Fields in ESR and VAR Processes, *Proc. of Liquid Metal Proccessing and Casting,* ed. P. D. Lee, A. Mitchell, J. Bellot, and A. Jardy*,* 205-214*,* 2003.
8. Yu Kuang-O, Comparison of ESR-VAR Processes – Part 1, Heat Transfer Characteristics of Crucible, *Proc. Vacuum Metallurgy Conference.,* ed. G.K Bhat and L.W. Lherbier, pp. 83-92, 1984.
9. Bertram L.A., Adasczik C.B, Evans D.G., Minisandram R.S., Sackinger P.A., Wegman D.D., Williamson R.L., Quantitative Simulations of Superalloy VAR Ingot at the Macroscale, *Liquid Metal Processing and Casting*, ed. A. Mitchell and P. Aubertin, AVS, 110-132, 1997.
10. B.E. Launder and D.B. Spalding, The Numerical Computation of Turbulent Flow, *Comp. Meth. in Appl. Mech. and Eng*., 3, 269-281, 1974.
11. S.V. Patankar, *Numerical Heat Transfer and Fluid Flow*, Hemisphere Publishing Corporation, Washington, 1980.
12. COMPACT-ESR Reference Manual, Innovative Research, Inc., 3025 Harbor Lane N., Suite 300, Plymouth, MN 55447, www.inres.com, 2005.
13. S. Viswanathan, *Private Communication*, Sandia National Laboratories, Albuquerque, NM 87123, 2004.